Graded SiGe Channel Dielectric Modulated Tunnel FET Bio Sensor: Proposal And Comparative Analysis

Komal Kumari , Sharmistha Shee Kanrar, Abir Jana, Tapas Chakraborty, and Subir Kumar Sarkar

Jadavpur University (Dept. ETCE), Kolkata, India.

This study presents a novel approach utilizing a Graded SiGe Tunnel Field-Effect Transistor (Gr.SiGe-TFET) for the development of a high-performance ultrathin biosensor for label-free biomolecule detection. The study addresses the challenges of hereto-junction TFETs by achieving reasonably high current through the utilization of graded SiGe in a Ge-SiGe-Si structure, substantiating its superiority through comparisons with Ge-Ge-Si , Ge-Si-Si , Ge-$Si_{0.5}Ge_{0.5}$-Si structures. The paper includes theoretical analysis to substantiate the simulation findings for dielectric constant values (k=2,4,6,9,12) corresponding to biomolecules such as Biotin, Ferro-cytochrome, Bacteriophage T7, Keratin, and Gelatin. We performed comprehensive analysis of sensitivity and selectivity with various target biomolecules, characterized by different dielectric constants, using calibrated TCAD simulations. Our findings show that the proposed SiGe graded channel biosensor (Ge-Gr.SiGe-Si structure) has optimized sensitivity compared to Ge-Ge-Si , Ge-Si-Si , Ge-$Si_{0.5}Ge_{0.5}$-Si structures making it a strong candidate for biosensors.

Keywords- Biosensor, Dielectric Modulation, Graded SiGe, Tunnel FET.

INTRODUCTION

In recent years, the demand for high-performance biosensors has grown significantly, driven by the need for sensitive and reliable detection methods in healthcare, environmental monitoring, and food safety. Researchers have been exploring innovative device architectures and materials to enhance sensor performance. Biosensors can be classified based on their transduction mechanisms, including electrochemical biosensors (e.g., genic sensors), electronic biosensors (such as various FETs like MOSFETs, ISFETs, and TFETs), and gravimetric biosensors (thermal and acoustic sensors) [1]. Among these, electronic biosensors stand out for their established fabrication technologies, CMOS compatibility, and integrability with standard ICs. Field-Effect Transistors (FETs) are particularly attractive for label-free detection due to their scalability, cost-effectiveness, and ability to integrate sensors and measurement systems on a chip [2-3].

Tunnel Field-Effect Transistors (TFETs) are promising candidates for biosensors, offering advantages like lower subthreshold swing (SS), reduced ambipolar characteristics, and high

sensitivity through tunneling mechanisms [4-8]. Scaling to sub-10 nm demands alternative channel, source, and pocket materials to meet IRDS drive current limits [9]. Germanium (Ge), with its low bandgap and high hole mobility, is a strong candidate [10-11]. As a pseudo-direct bandgap material, Ge offers enhanced band-to-band tunneling (BTBT) efficiency compared to Si [12]. Kim et al. demonstrated that Si-Ge-Si TFETs outperform Si-Si-Si and Ge-Ge-Ge counterparts due to optimized tunneling resistance and reduced ambipolarity at the Ge/Si heterojunctions [13]. However, pure Ge-based devices face challenges such as lattice mismatch with Si and integration complexities [14].

Graded SiGe channels address these challenges by maximizing transconductance and improving performance [15]. Early SiGe FETs with SiO_2 insulation and $TiSi_2$ Schottky gates mitigated gate leakage and enhanced hole mobility through spacer layers [16]. Advances like hybrid SiGe-channel CMOS and SiGe-based FINFETs achieved high speeds and scalability for 10 nm nodes [17-18]. $Si_{0.8}Ge_{0.2}$ and $Si_{0.5}Ge_{0.5}$ graded channels demonstrated improved ON currents, reduced OFF currents, and better SS compared to Si-based devices [19-20]. However, vertical grading faces limitations in scalability and stability, constrained by critical layer thickness and defect formation [15, 21-22]. Recently, Lee et al. fabricated a CMOS-compatible gate-all-around SiGe TFET with high Ge content ($Si_{0.2}Ge_{0.8}$) and achieved remarkable SS and low leakage current [23].

To overcome performance degradation from defects and ambipolarity, this study proposes a Graded SiGe Tunnel Field-Effect Transistor (Gr.SiGe-TFET) biosensor. By incorporating graded SiGe layers in a Ge-SiGe-Si configuration, the structure addresses key TFET challenges, ensuring high sensitivity and stable performance. Shih et al. showed graded Si/Ge TFETs optimize tunneling barriers for ON/OFF switching and suppress short-channel effects in sub-10 nm devices, but scaling challenges persist with ambipolarity [24]. This study proposes an ultrathin biosensor using a Gr.SiGe-TFET highlighting its advantages in label-free biomolecule detection. The paper is organized as follows: Section II details the device architecture and simulation methodologies. Section III analyzes the device's electrostatic properties and sensitivity, and Section IV summarizes findings and implications.
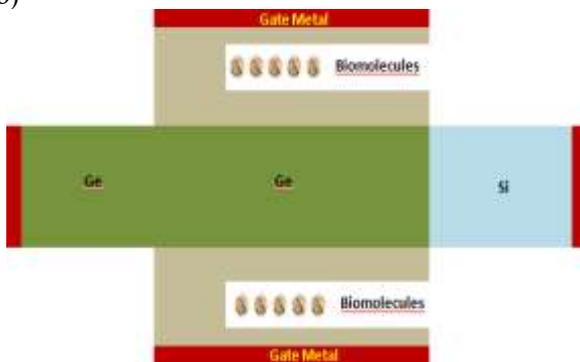
II: DEVICE STRUCTURE , THEORITICAL FOUNDATION , SIMULATION ASPECTS
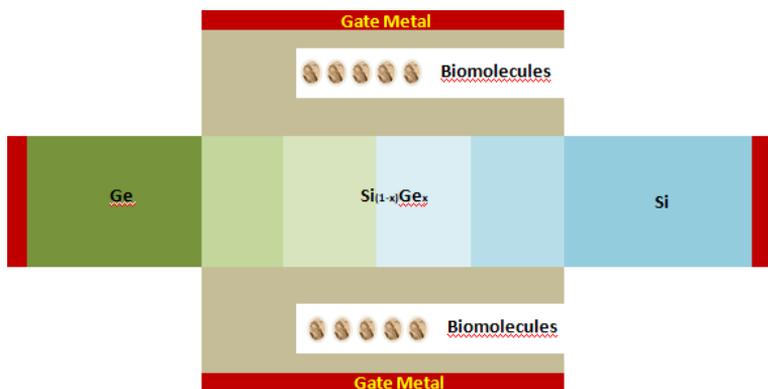
(a)
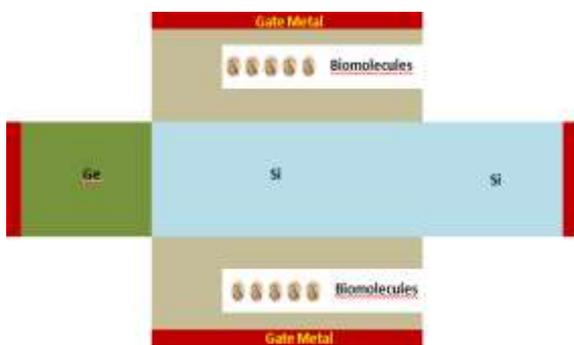
(b)

(c)

(d)

Fig. 1. (a) schematic picture of proposed graded channel TFET biosensor (b) Ge-Si-Si, (c) Ge-Ge-Si, (d) Ge-Si$_{0.5}$Ge$_{0.5}$-Si structures for comparative analysis

A schematic presentation of the device structure is given in Figure 1. The Parameters employed in the proposed device for modeling and simulation purposes are given in Table I.

Parameters	Value
Source Length	10 nm
Intrinsic Channel Length	40 nm
Drain Length	10 nm
Thickness of Channel (t_{SiGe})	10 nm
Thickness of oxide layer (t_{ox})	1 nm
Device width (W)	20 nm
Work function of the gate metal (φm)	4.45 eV
Source region Concentration	$10^{20}(p)$
Intrinsic Chennel Concentration	$10^{16}(p)$cm-3
Drain Pocket Concentration	$10^{14}(p)$cm-3
Drain region Concentration	$10^{18}(n)$cm-3

Table 1: Parameters utilized in the proposed device for modeling and simulation purposes.

For the device shown in figure 1, the 2-D Poisson equation is as follows:

$$:\frac{\partial^2\varphi(x.y)}{\partial x^2} + \frac{\partial^2\varphi(x.y)}{\partial y^2} = \frac{qn}{\epsilon_{ch}}, \qquad \text{i=1,2,3,4, 5 as regions depicted in figure 1}$$

$$(1)$$

$\varphi(x.y)$ is the two dimensional potential, n and q are the carrier density and charge, ϵ_{ch} is the dielectric permittivity .

From figure 1, the region i denotes the different region in the channel. By Young's Parabolic approximation

$$\varphi_i(x, y) = \varphi_{s,i}(x) + ya_{1i}(x) + y^2 a_{2i}(x) \qquad i=1,2,3,4,5$$

(2)

Where $\varphi_i(x, y)$ *is* 2-D potential profile , $a_i(x)$ is one dimensional potential along length. To calculate a_0, a_{1i} *and* a_{2i} we apple the boundary conditions as:-

1) $at\ y = 0, \varphi_i(x, y) = \varphi_{s,i}(x)$

2) $\dfrac{\partial \varphi_i(x,y)}{\partial y}\Big|_{y=0} = a_{1i}(x)$

(3)

3) $\dfrac{\partial \varphi_i(x,y)}{\partial y}\Big|_{y=t(Si_{(1-mfi)}\ Ge_{(mfi)})} = a_{1i}(x) + 2t_{Si_{(1-mfi)}Ge_{(mfi)}}a_{2i}(x)$

$\varphi_{s,i}(x)$ is the surface potential, $t(Si_{(1-mfi)}Ge_{(mfi)})$ is the thickness of the graded channel. 'mfi' denotes the Germanium mole fraction in Silicon in each region. Solving,

$$a_{2i}(x) = \frac{C_{ox}[V_{GS}-V_{fbi}-\varphi_{s,i}]}{t_{Si_{(1-mfi)}\ Ge_{(mfi)}}\epsilon_{Ge/Si_{(1-mfi)}\ Ge_{(mfi)}}}, \quad a_{1i}(x) = \frac{-C_{ox}[V_{GS}-V_{fbi}-\varphi_{s,i}]}{t_{Si_{(1-mfi)}\ Ge_{(mfi)}}\epsilon_{Ge/Si_{(1-mfi)}\ Ge_{(mfi)}}}$$

(4)

V_{GS} is the gate to source voltage, V_{fbi} is the flat-band voltage corresponding to every region, ϵ is the permittivity. C_{ox} is the oxide capacitance . Now 1-D equation takes the form,

$$\frac{\partial^2 \varphi_{s,i}(x)}{\partial x^2} - \frac{\varphi_{s,i}(x)-(V_{GS}-V_{fbi})}{\lambda_i^2} = \frac{qN_i}{\epsilon_{Ge/Si_{(1-mfi)}\ Ge_{(mfi)}}}$$

(5)

λ_i is the characteristics length given by, $\lambda_i = \sqrt{\dfrac{t_{Ge/Si_{(1-mfi)}Ge_{(mfi)}}\epsilon_{Si_{(1-mfi)}Ge_{(mfi)}}}{2C_{HfO2}}}$

(6)

Here, $2/\pi$ is multiplied in the denominator to consider fringing field effects.

The general solution of the above differential equation,

$$\varphi_{S,i}(x) = \alpha_i\, exp\left(\frac{x}{\lambda_i}\right) + \beta_i\, exp\left(-\frac{x}{\lambda_i}\right) + \sigma_i, \text{ Where, } \sigma_i = V_{GS} - V_{fb,i} - \frac{qN_i}{\epsilon_{Ge/Si_{(1-mfi)}Ge_{(mfi)}}}\lambda_i^2,$$

(7)

In this study, we have simulated four distinct TFET structures to analyze their performance as biosensors: Ge-Ge-Si, Ge-SiGe graded-Si (denoted as Ge_Gr.SiGe_Si), Ge-Si$_{0.5}$Ge$_{0.5}$-Si, and

Ge-Si-Si as shown in figure 1(c). Each structure represents a unique approach to enhancing tunneling efficiency and sensitivity to dielectric modulation. The Ge-Ge-Si configuration utilizes a heterojunction with abrupt transitions, while the Ge-Si-Si structure incorporates a conventional Si drain. The Ge-Si$_{0.5}$Ge$_{0.5}$-Si design introduces an intermediate SiGe layer for smoother bandgap alignment, and the Ge-SiGe graded-Si structure employs a graded composition to minimize lattice mismatch and optimize band-to-band tunneling. These structures are modeled to explore their potential for high-sensitivity biosensing, focusing on their dielectric modulation response and overall electrostatic control. To analysze the device characteristics, ATLAS Silvaco had been applied in the simulation. Along with local BTBT model, FD statistics , DD carrier transport, SRH recombination model, bandgap narrowing are employed. Kane's mode is used to calculate Band to band tunneling generation rate at uniform electric field where [13] P is considered 2.5 for indirect tunneling and calibrated [23]. For the simulation environment, we have considered dielectric constant values (k=2,4,6,9,12) corresponding to biomolecules such as Biotin, Ferro-cytochrome, Bacteriophage T7, Keratin, and Gelatin[25].

From fabrication aspect, the arrangement can be grown on a silicon substrate followed by the layers of graded SiGe and SiO$_2$ for gate oxide, respectively. From a fabrication aspect, The possible fabrication process begins with SOI substrates, where initial characterization using nano-beam and X-ray diffraction confirms minimal strain. Selective epitaxial growth methods are generally used for the formation of SiGe and Si layers with specific grading profiles. Ultrahigh vacuum chemical vapor deposition (UHV-CVD) is employed for selective epitaxial growth [26]. Subsequently, gate dielectric is generally formed via rapid thermal oxidation. Dopants at source/drain are implanted followed by activation with rapid thermal annealing where cavities can be etched out by buffered HF. The development of materials with precise compositional is achieved such as chemical vapor deposition, metal-assisted vapor-liquid-solid (VLS) growth techniques, laser ablation with thermal evaporation and dynamic shadowing deposition [27-32]. Experimentally, the lower heat conductivity of Si/Si$_{1-x}$Ge$_x$ superlattices (SLs) with compositional gradients has been observed both in theory and in practice [33]. Zhang et al showed through MD simulations that the heat conductivity of compositionally graded SiGe nanowires (NWs) can decrease by as much as 57% when contrasted with SiGe NWs featuring sharp interfaces [27]. They introduced a compositional gradient ranging from 90% to 50% and 10% to 50% in the area near the SiGe interface.
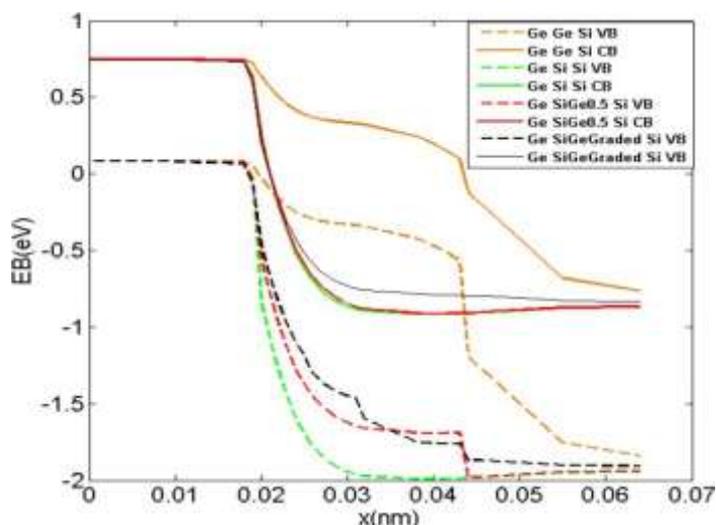
IV. RESULT AND DISCUSSION

Figure 1: Energy band diagram of the proposed Graded SiGe channel Dielectric Modulated Tunnel FET BioSensor.

In the context of the Graded SiGe channel Dielectric Modulated Tunnel FET BioSensor, the energy band diagram reveals significant variations in tunneling distance based on different configurations. The Ge-Ge-Si configuration offers the highest tunneling distance due to the substantial bandgap difference between the Ge source and the Si drain, which creates a more substantial potential barrier for electrons to tunnel through. In contrast, configurations such as Ge_Gr.SiGe_Si, Ge-Si$_{0.5}$Ge$_{0.5}$-Si, and Ge-Si-Si exhibit shorter tunneling distances. This is because the graded SiGe layers and the intermediate Si$_{0.5}$Ge$_{0.5}$ layer in these configurations provide a more gradual transition in the energy band, reducing the overall potential barrier height and width. Consequently, the electrons encounter a narrower and less abrupt barrier, facilitating easier tunneling. The Ge-Si-Si structure, while also having a significant bandgap difference, presents a relatively moderate tunneling distance compared to Ge-Ge-Si due to the direct Ge to Si transition without the intermediate graded layer, resulting in a different tunneling profile. The varied tunneling distances directly impact the device's performance, affecting the ON-state current and the overall efficiency of the TFET BioSensor.
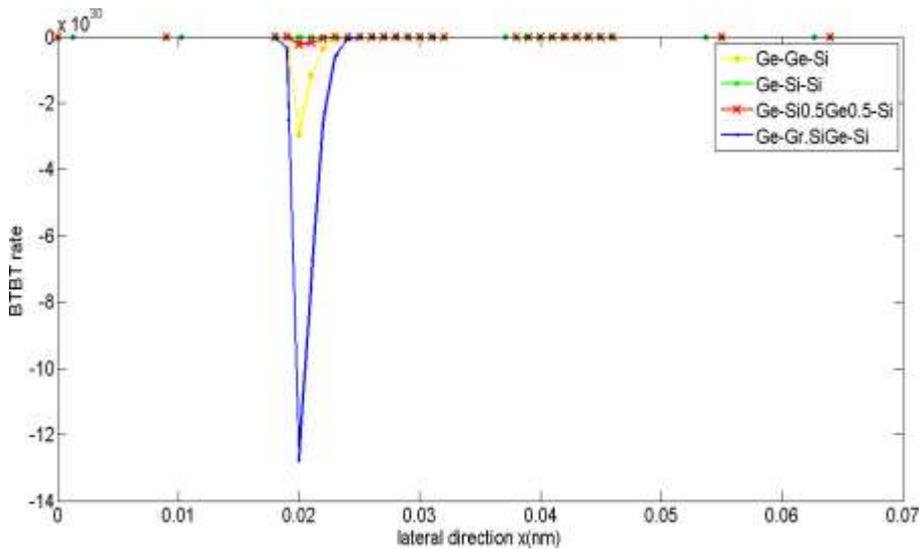
Figure 2: BTBT plot comparing the tunneling current at the source side for various configurations using the local tunneling model.
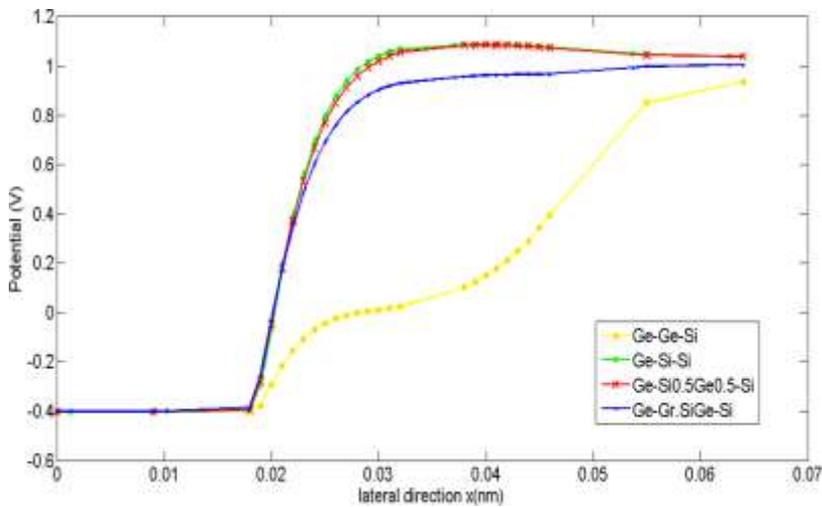

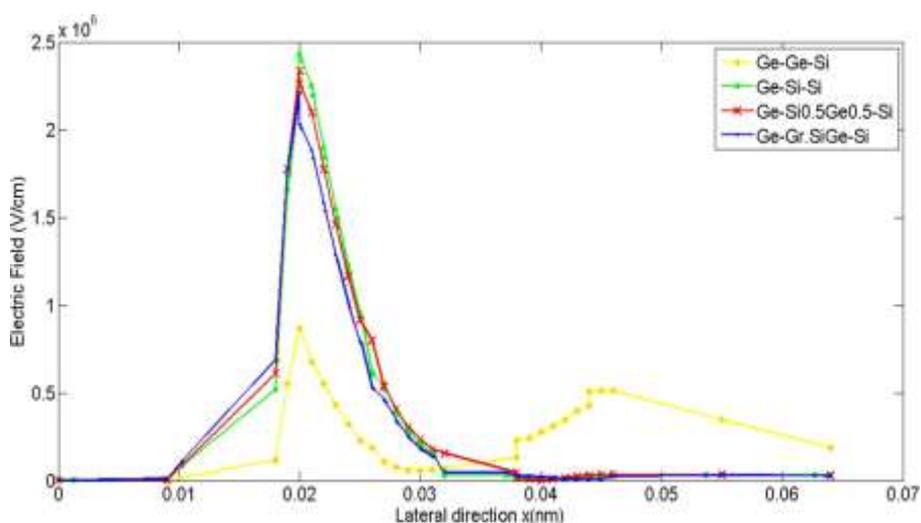Figure 3: Potential Energy Curves for Different Semiconductor Structures

Figure 4: Electric field distribution in TFETs showing the impact of different semiconductor structures
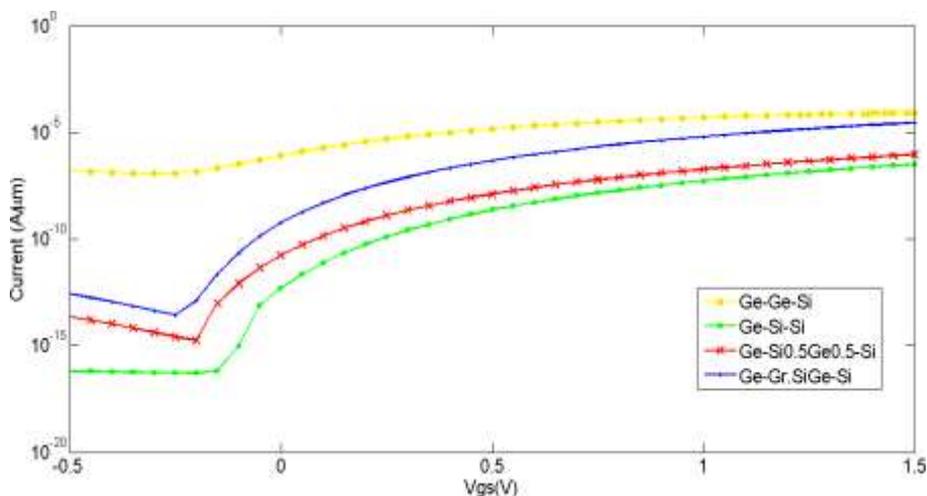

Figure 5: Current drain voltage graph illustrating the trade-offs between Ion/Ioff ratio, ambipolarity, and on-current for various SiGe graded structures
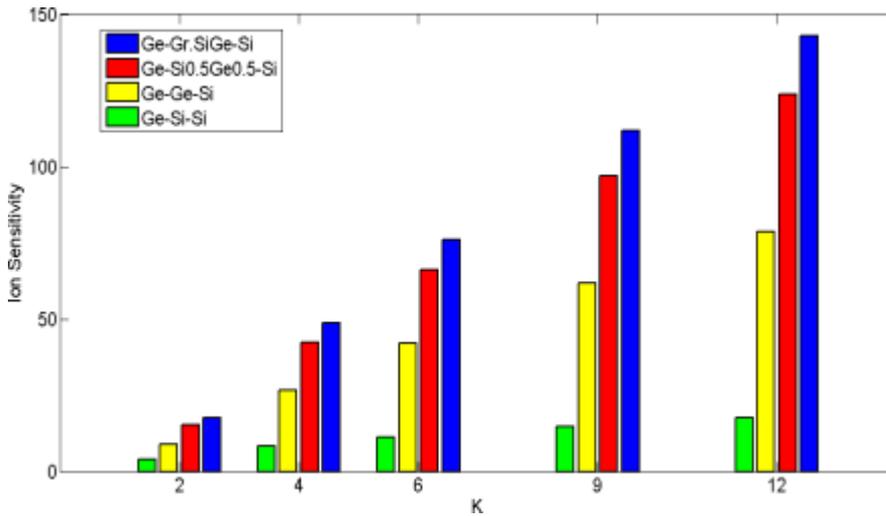
Figure 6: Comparison of Ion sensitivity between Ge-Ge-Si, Ge-Si-Si , Ge- $Si_{0.5}Ge_{0.5}$-Si, and Ge_Gr.SiGe_Si - models as a function of biosensor permittivity.

A comparative analysis in figure 2 shows the rate of increase in BTBT follows the sequence: Ge-Si-Si, Ge-$Si_{0.5}Ge_{0.5}$-Si, Ge-Ge-Si, and Ge_Gr.SiGe_Si. The Ge-Si-Si configuration exhibits the steepest increase in BTBT due to its abrupt transition, which creates a significant potential barrier that enhances tunneling rates. In the Ge- Ge-$Si_{0.5}Ge_{0.5}$-Si -Si and Ge-Ge-Si configurations, intermediate SiGe layers smooth the potential transition, reducing the tunneling barrier and moderating the BTBT rate compared to Ge-Si-Si. The Ge_Gr.SiGe_Si structure further improves tunneling efficiency due to its gradual potential variation, enhancing the process more effectively.

The potential energy curves illustrate the variations across different semiconductor interfaces, highlighting their impact on strain relaxation and defect dynamics. The Ge-Ge-Si structure shows a smoother potential rise due to similar lattice constants but struggles with managing strain and defects, affecting performance. In contrast, the Ge-Si-Si and Ge-$Si_{0.5}Ge_{0.5}$-Si structures exhibit sharp potential changes, resulting in high strain, lattice mismatch, and a greater propensity for threading dislocations (TDs) and other defects. The Ge_Gr.SiGe_Si structure, with its gradual Ge mole fraction transition, effectively reduces lattice mismatch and strain, minimizing defects and improving the crystal quality of the Ge-$Si_{0.5}Ge_{0.5}$-Si channel layer.

Figure 4 shows the electric field distribution across different structures, with the sharpest increase near the source for Ge-Si-Si, enhancing tunneling but increasing defect risks. The Ge_Gr.SiGe_Si structure displays a smoother electric field profile, reducing lattice mismatch and strain, thus lowering defect density and improving reliability. This balance makes the Ge_Gr.SiGe_Si structure particularly advantageous for integrating high-mobility SiGe channels in advanced devices, enabling better performance and scalability.

The current drain voltage graph in figure 5 reveals that the Ge-Si-Ge structure has the lowest Ion/Ioff ratio, indicating poor on-off current differentiation. The Ge-Si-Si structure, while exhibiting the lowest ambipolarity, fails to produce significant on-current due to less effective carrier transport. In contrast, the Ge-Si$_{0.5}$Ge$_{0.5}$-Si structure shows higher ambipolarity but also higher on-current, as the presence of Ge enhances carrier mobility, increasing current. The Ge_Gr.SiGe_Si structure strikes a balance by optimizing the Ion/Ioff ratio, providing improved performance with an increase in ambipolarity similar to the Ge-Si$_{0.5}$Ge$_{0.5}$-Si structure. This optimization is attributed to the graded SiGe layer, which effectively manages strain and reduces defects, facilitating better tunneling and carrier transport, thereby enhancing TFET operation.

In figure 6, the Ion sensitivity of the proposed biosensor structures was evaluated for dielectric constants (k=2,4,6,9,12), with the results highlighting distinct performance trends. The Ge-Ge-Si structure exhibited moderate sensitivity, with values of 8.97, 26.58, 42.02, 61.81, and 78.60, respectively. Its sensitivity increases with k due to efficient tunneling at the Ge/Si heterojunction but is limited by higher ambipolarity and abrupt band transitions. The Ge-Si-Si configuration showed the lowest sensitivity, with values of 3.85, 8.26, 11.25, 14.70, and 17.49, resulting from significant tunneling resistance due to abrupt Ge/Si and Si/Si interfaces, which hinder BTBT efficiency. The Ge-Si$_{0.5}$Ge$_{0.5}$-Si structure provided significantly higher sensitivity, with values of 15.31, 42.42, 66.08, 96.91, and 123.63, benefiting from the intermediate SiGe layer that smoothens the bandgap transition and reduces tunneling resistance. The highest sensitivity was observed in the Ge_Gr.SiGe_Si structure, with values of 17.47, 48.70, 76.09, 111.84, and 142.79, due to its graded composition, which creates a continuous potential barrier, minimizes lattice mismatch, and reduces defect density. This design ensures enhanced tunneling efficiency and amplifies the device's response to dielectric variations, making it the most suitable for high-sensitivity biosensing applications

For selectivity of k=2 with respect to other bimolecular dielectricity, Ge-Si-Si achieves the highest values 46.57, Ge-Gr.SiGe-Si shows slightly lower but comparable values to Ge-Si$_{0.5}$Ge$_{0.5}$-Si, indicating its effectiveness in low-dielectric environments. Ge-Ge-Si shows consistently lower selectivity compared to graded structures, with a steep decline as k increases. For selectivity of k=4 the Ge-Ge-Si structure demonstrates the highest selectivity for k=4/2 (296.27), followed by Ge-Si$_{0.5}$Ge$_{0.5}$-Si (277.13) and Gr.SiGe-Si (278.59) emphasizing their suitability for intermediate contrasts. For Selectivity of k=6, Gr.SiGe-Si and Ge-Si$_{0.5}$Ge$_{0.5}$-Si alternate as the best performers in this range, with near-identical selectivity values for all k. Ge-Ge-Si and Ge-Si-Si shows weaker performance in this range. For Selectivity of k=9 and k=12, Graded SiGe-Si and Ge-Si$_{0.5}$Ge$_{0.5}$-Si consistently outperform others in high dielectric contrast scenarios. For k=12/2, the Graded SiGe-Si structure achieves the highest selectivity (815.71), followed closely by Ge-Si$_{0.5}$Ge$_{0.5}$-Si (807.54). Ge-Ge-Si performs well in extreme ratios but shows a sharper decline in intermediate ranges. Ge-Si-Si remains the weakest across all high-dielectric contrast cases due to its abrupt interfaces and limited electrostatic control. Graded and intermediate SiGe structures show superior scalability, sensitivity and maintain consistent performance across all k..

The below mentioned data compares the **selectivity values** (defined as the ratio of sensitivities) of four TFET-based biosensor structures—**Ge-Ge-Si**, **Ge-Si-Si**, **Ge-Si₀.₅Ge₀.₅-Si**, and **Graded SiGe-Si**—under various dielectric constant (k) ratios.

Table 2: Selectivity for k=2 with respect to BacteriophageT7,6,9,12.

	Selectivity with respect to k=4	Selec Selectivity with respect to k= 6	Selectivity with respect to k=9	Selectivity with respect to k=12
Ge –Ge- Si	33.75278	21.34846	14.51167	11.41209
Ge -Si -Si	46.56948	34.19523	26.18202	22.00104
Ge - Si₀.₅Ge₀.₅ - Si	36.08461	23.16738	15.79636	12.38329
Ge -Gr. SiGe -Si	35.89538	22.9855	15.64552	12.25922

	Selectivity with respect to k=2	Selectivity with respect to k=6	Selectivity with respect to k=9	Selectivity with respect to k=12
Ge –Ge- Si	296.2719	63.24948	42.99399	33.81081
Ge -Si -Si	214.7329	73.42842	56.22142	47.24348
Ge -Si₀.₅Ge₀.₅ -Si	277.1265	64.20295	43.7759	34.31739
Ge -Gr. SiGe -Si	278.5874	64.03472	43.58644	34.15265

Table 3: Selectivity for k=4 with respect to k=4, 6,9,12.

	Selectivity with respect to k=2	Selectivity with respect to k=4	Selectivity with respect to k=9	Selectivity with respect to k=12
Ge –Ge- Si	468.4179	158.1041	67.97524	53.45626
Ge -Si - Si	292.4385	136.1871	76.5663	64.33951
Ge - Si₀.₅Ge₀.₅ -Si	431.6414	155.7561	68.18362	53.45142
Ge -Gr. SiGe -Si	435.0568	156.1653	68.06688	53.33457

Table 4: Selectivity for k=6 with respect to k=2,4,9,12.

	Selectivity with respect to k=2	Selectivity with respect to k=4	Selectivity with respect to k=6	Selectivity with respect to k=12
Ge –Ge-Si	689.1007	232.5907	147.1124	78.64078
Ge -Si -Si	381.9415	177.8681	130.6058	84.03111
Ge -Si$_{0.5}$Ge$_{0.5}$ -Si	633.0572	228.4362	146.6628	78.39334
Ge -Gr. SiGe -Si	639.1608	229.4292	146.9143	78.35613

Table 5: Selectivity for k=9 with respect to k=2,4,6,12.

	Selectivity with respect to k=2	Selectivity with respect to k=4	Selectivity with respect to k=6	Selectivity with respect to k=9
Ge –Ge-Si	876.2639	295.7634	187.0688	127.1605
Ge -Si -Si	454.5239	211.6694	155.4255	119.0036
Ge -Si$_{0.5}$Ge$_{0.5}$ -Si	807.5396	291.3975	187.0858	127.5619
Ge -Gr. SiGe -Si	815.7126	292.8031	187.4957	127.6224

Table 6: Selectivity for k=12 with respect to K= 2, 4,6,9.

V.   CONCLUSION

In conclusion, this study examines the impact of different semiconductor structures and modeling approaches on the performance of advanced tunnel field-effect transistors (TFETs) and biosensors. The analysis of structures such as Ge-Ge-Si, Ge-graded SiGe-Si (Ge_Gr.SiGe_Si) , Ge- Si$_{0.5}$Ge$_{0.5}$-Si, and Ge-Si-Si highlights their distinct effects on tunneling efficiency, defect density, and carrier mobility. Among these, the graded SiGe buffer structure demonstrates significant advantages by minimizing lattice mismatch, reducing defect formation, and enhancing carrier transport efficiency. This structural optimization improves electrical characteristics, making the Ge_Gr.SiGe_Si configuration particularly suitable for integrating high-mobility channels in future semiconductor technologies. Additionally, the sensitivity of the SiGe graded channel biosensor can be enhanced by optimizing Ge content, channel doping, and geometry to suit biomolecules with different dielectric constants (ε). The Graded SiGe-Si and Ge-Si$_{0.5}$Ge$_{0.5}$-Si structures demonstrate superior selectivity overall, attributed to their smooth bandgap transitions and enhanced electrostatic control. Among these, Graded SiGe-Si excels at high dielectric contrasts, due to its continuous composition and minimized defect density. In contrast, the Ge-Ge-Si and Ge-Si-Si structures perform weaker, with abrupt transitions and limited adaptability to varying dielectric environments

hindering their selectivity and overall sensitivity. This research provides practical insights into optimizing TFETs and biosensors for next-generation applications.

REFERENCES

[1]Varnakavi. Naresh and N. Lee, "A Review on Biosensors and Recent Development of Nanostructured Materials-Enabled Biosensors," Sensors, vol. 21, no. 4, p. 1109, Feb. 2021, doi: https://doi.org/10.3390/s21041109.

[2]D. Sarkar and K. Banerjee, "Fundamental limitations of conventional-FET biosensors: Quantum-mechanical-tunneling to the rescue," 70th Device Research Conference, University Park, PA, USA, 2012, pp. 83-84, doi: 10.1109/DRC.2012.6256950. keywords: {Sensitivity;Biosensors;Photonic band gap;Tunneling;Dielectrics;Time factors;Doping},

[3]R. Misra, K. Singh, A. Agarwal, R. Rastogi, and S. Dubey, "Electronic Noise Analysis of Source-Engineered Phosphorene/Si Heterojunction Dopingless Tunnel-FET," Silicon, vol. 15, no. 1, pp. 263–267, Jul. 2022, doi: https://doi.org/10.1007/s12633-022-02019-5.

[4]Sarkar, S.; Banerjee, K. Fundamental limitations of conventional-FET biosensors: Quantum-mechanical-tunneling to the rescue. In Proceedings of the 70th Device Research Conference, University Park, PA, USA, 18–20 June 2012; pp. 83–84. [Google Scholar] [CrossRef]

[5]Narang, R.; Reddy, K.V.S.; Saxena, M.; Gupta, R.S.; Gupta, M. A Dielectric-Modulated Tunnel-FET-Based Biosensor for Label-Free Detection: Analytical Modeling Study and Sensitivity Analysis. IEEE Trans. Electron Devices 2012, 59, 2809–2817. [Google Scholar] [CrossRef]

[6]Narang, R.; Saxena, M.; Gupta, R.S.; Gupta, M. Dielectric Modulated Tunnel Field-Effect Transistor—A Biomolecule Sensor. IEEE Electron Device Lett. 2012, 33, 266–268. [Google Scholar] [CrossRef]

[7]Kanungo, S.; Chattopadhyay, S.; Gupta, P.S.; Rahman, H. Comparative Performance Analysis of the Dielectrically Modulated Full-Gate and Short-Gate Tunnel FET-Based Biosensors. IEEE Trans. Electron Devices 2015, 62, 994–1001. [Google Scholar] [CrossRef]

[8]Anam, A.; Anand., S.; Amin, S.I. Design and Performance Analysis of Tunnel Field Effect Transistor with Buried Strained Si1−xGex Source Structure Based Biosensor for Sensitivity Enhancement. IEEE Sens. J. 2020, 20, 13178–13185. [Google Scholar] [CrossRef]].

[9]Arimura, E. Capogreco, A. Vohra et al., (2020) Toward high-performance and reliable Ge channel devices for 2 nm node and beyond. In: 2020 IEEE International Electron Devices Meeting (IEDM). IEEE, San Francisco, CA, USA, p 2.1.1–2.1.4

[10]J. Mitard, L. Witters, Y. Sasaki et al., (2016) A 2nd Generation of 14/16nm-node compatible strained-Ge pFINFET with improved performance with respect to advanced Si-channel FinFETs. In: 2016 IEEE Symposium on VLSI Technology. pp 1–2

[11]Y. Li, F. Zhao, X. Cheng et al., Integration of Si0. 7Ge0. 3 fin onto a bulk-Si substrate and its P-type FinFET device fabrication. Semicond. Sci. Technol. 36, 125001 (2021)

[12]Maximilian Georg Bartmann et al., "Verifying the band gap narrowing in tensile strained Ge nanowires by electrical means," Nanotechnology, vol. 32, no. 14, pp. 145711–145711, Jan. 2021, doi: https://doi.org/10.1088/1361-6528/abd0b2.

[13]Kim, G.; Lee, J.; Kim, J.H.; Kim, S. High On-Current Ge-Channel Heterojunction Tunnel Field-Effect Transistor Using Direct Band-to-Band Tunneling. Micromachines 2019, 10, 77. https://doi.org/10.3390/mi10020077

[14]L. Witters, G. Eneman, J. Mitard et al., Integration aspects of strained Ge pFETs. Solid State Electron. 98, 7–11 (2014). https://doi.org/10.1016/j.sse.2014.04.009

[15]S. Verdonckt-Vandebroek et al., "SiGe-channel heterojunction p-MOSFET's," in IEEE Transactions on Electron Devices, vol. 41, no. 1, pp. 90-101, Jan. 1994, doi: 10.1109/16.259625.

[16]K. Cheng et al., "High performance extremely thin SOI (ETSOI) hybrid CMOS with Si channel NFET and strained SiGe channel PFET," 2012 International Electron Devices Meeting, San Francisco, CA, USA, 2012, pp. 18.1.1-18.1.4, doi: 10.1109/IEDM.2012.6479063.

[17]D. Guo et al., "FINFET technology featuring high mobility SiGe channel for 10nm and beyond," 2016 IEEE Symposium on VLSI Technology, Honolulu, HI, USA, 2016, pp. 1-2, doi: 10.1109/VLSIT.2016.7573360.

[18]C. H. Lee et al., "Toward High Performance SiGe Channel CMOS: Design of High Electron Mobility in SiGe nFinFETs Outperforming Si," 2018 IEEE International Electron Devices Meeting (IEDM), San Francisco, CA, USA, 2018, pp. 35.1.1-35.1.4, doi: 10.1109/IEDM.2018.8614581.

[19]C.-J. Sun et al., "Low Ge Content Ultra-Thin Fin Width (5nm) Monocrystalline SiGe n-Type FinFET With Low Off State Leakage and High ION/IOFF Ratio," IEEE Journal of the Electron Devices Society, vol. 8, pp. 1016–1020, 2020, doi: https://doi.org/10.1109/jeds.2020.3023953.

[20] Y. Li et al., "A novel approach to Si0.5Ge0.5 channel FinFET fabrication: utilizing a three-layer SiGe strain relaxation buffer and In-Situ phosphorus doping," Journal of materials science. Materials in electronics, vol. 35, no. 6, Feb. 2024, doi: https://doi.org/10.1007/s10854-024-12174-7.

[21]B. Vincent et al., "The Ge condensation technique: A solution for planar SOI/GeOI co-integration for advanced CMOS technologies?," Materials science in semiconductor processing, vol. 11, no. 5–6, pp. 205–213, Oct. 2008, doi: https://doi.org/10.1016/j.mssp.2008.10.005.

[22]N. D. Chien, "Design Optimization Of Extremely Short-Channel Graded Si/Sige Heterojunction Tunnel Field-Effect Transistors For Low Power Applications," Vietnam Journal of Science and Technology, vol. 51, no. 6, p. 757, Mar. 2018, doi: https://doi.org/10.15625/2525-2518/51/6/11642.

[23] R. Lee et al., "Vertically-Stacked Si0.2Ge0.8 Nanosheet Tunnel FET With 70 mV/Dec Average Subthreshold Swing," in IEEE Electron Device Letters, vol. 42, no. 7, pp. 962-965, July 2021, doi: 10.1109/LED.2021.3079246.

[24]C. Shih and Nguyễn Đăng Chiến, "Physical operation and device design of short-channel tunnel field-effect transistors with graded silicon-germanium heterojunctions," Journal of Applied Physics, vol. 113, no. 13, Apr. 2013, doi: https://doi.org/10.1063/1.4795777.

[25] S. Choudhury, Krishna Lal Baishnab, K. Guha, Zoran Jakšić, O. Jakšić, and J. Iannacci, "Modeling and Simulation of a TFET-Based Label-Free Biosensor with Enhanced Sensitivity," vol. 11, no. 5, pp. 312–312, May 2023, doi: https://doi.org/10.3390/chemosensors11050312.

[26]Grace Huiqi Wang, E.-H. Toh, C.-H. Tung, S. Tripathy, G. S. Samudra, and Y.-C. Yeo, "Concept of Strain-Transfer-Layer and Integration with Graded Silicon–Germanium Source/Drain Stressors for p-Type Field Effect Transistor Performance Enhancement," Japanese journal of applied physics, vol. 47, no. 4S, pp. 2551–2551, Apr. 2008, doi: https://doi.org/10.1143/jjap.47.2551.

[27] H. Zhang, H. Han, S. Xiong, H. Wang, S. Volz, and Y. Ni, "Impeded thermal transport in composition graded SiGe nanowires," Appl. Phys. Lett., vol. 111, no. 12, Sep. 2017, doi: 10.1063/1.4998998.

[28] T. Kuykendall, P. Ulrich, S. Aloni, and P. Yang, "Silicon-germanium nanowires," Nat. Mater., vol. 6, pp. 951, 2007.

[29] Y. Liu, J. A. Zapien, Y. Y. Shan, C. Y. Geng, C. S. Lee, and S. T. Lee, "Synthesis and characterization of silicon-germanium nanowires," Adv. Mater., vol. 17, pp. 1372, 2005.

[30] A. Pan, R. Liu, M. Sun, and C. Ning, "Controlled synthesis of single crystalline silicon nanowires," ACS Nano, vol. 4, pp. 671, 2010.

[31] S. Larson and Y. Zhao, "Nanostructured materials for energy applications," Nanotechnology, vol. 27, no. 255401, 2016.

[32] Y. He, J. Fan, and Y. Zhao, "Alleviating strain in Ge films by organic-inorganic hybrid materials," Cryst. Growth Des., vol. 10, pp. 4954, 2010.

[33] P. Ferrandovillalba, A. F. Lopeandia, F. X. Alvarez, B. Paul, C. De Tomas, M. I. Alonso, M. Garriga, A. R. Goni, J. Santiso, G. Garcia, et al., "Nano-engineered materials for various applications," Nano Res., vol. 8, pp. 2833, 2015.